



Iron-copper bimetallic nanoparticles embedded within ordered mesoporous carbon as effective and stable heterogeneous Fenton catalyst for the degradation of organic contaminants

Yanbin Wang^a, Hongying Zhao^b, Guohua Zhao^{a,b,*}

^a School of Materials Science and Engineering, Tongji University, 4800 Caoan Road, Shanghai 201804, PR China

^b Department of Chemistry, Key Laboratory of Yangtze River Water Environment, Ministry of Education, Tongji University, 1239 Siping Road, Shanghai 200092, PR China

ARTICLE INFO

Article history:

Received 12 July 2014

Received in revised form

19 September 2014

Accepted 22 September 2014

Available online 28 September 2014

Keywords:

Ordered mesoporous carbon

Heterogeneous Fenton

Iron-copper bimetallic

Organic contaminants

ABSTRACT

Iron-copper bimetallic nanoparticles embedded within ordered mesoporous carbon composite catalyst (CuFe-MC) was synthesized via a “one-pot” block-copolymer self-assembly strategy. The catalyst was characterized by transmission electron microscopy (TEM), scanning electron microscopy (SEM), X-ray diffraction (XRD), etc. The results showed the catalyst was ordered 2D hexagonal mesostructure and iron-copper nanoparticles highly dispersed in the matrix of ordered mesoporous carbon. The composite was used as a heterogeneous Fenton catalyst and showed a promising application in the degradation of non-biodegradation organic contaminants. Eight organic compounds were chosen as model contaminants, such as phenol, bisphenol A (BPA), etc. Efficient total organic carbon (TOC) removal of each organic contaminant was achieved by using CuFe-MC as catalyst, which was higher than that by Fe²⁺ ion at the same reaction condition. BPA was selected to further investigate the high catalytic activity of CuFe-MC. CuFe-MC presented high adsorption capacity for BPA due to its high BET surface area (639 m² g^{−1}) and mesostructure. The results of BPA degradation showed that the catalytic activity of CuFe-MC was much higher than Fe-MC and Cu-MC. Electron spin resonance (ESR) and high performance liquid chromatography (HPLC) results indicated that the concentration of generated hydroxyl radicals (•OH) with CuFe-MC was much higher than Fe-MC and Cu-MC. The low iron leaching of CuFe-MC suggested its good stability. Moreover, it could be easily separated by using an external magnet after the reaction and remained good activity after being recycled for several times, demonstrating its promising long-term application in the treatment of wastewater.

© 2014 Elsevier B.V. All rights reserved.

1. Introduction

Classic homogeneous Fenton oxidation is one of the powerful and widely used Advanced Oxidation Processes (AOPs) for the treatment of wastewater containing recalcitrant organic pollutants, such as pesticides, organic synthetic dyes, pharmaceuticals and personal care products [1]. However, the major defect of homogeneous Fenton reaction is the involvement of a large amount of iron salts that are presented in the effluents and requiring an additional separation step to separate iron-containing sludge. Besides, the narrow pH range (pH 2–3) is another limitation for its application [2,3]. In order to tackle these problems, heterogeneous Fenton

catalysis has been developed and used as a promising alternative for which the principal goal is the development of efficient and stable solid catalysts. Various solid catalysts, e.g., nano zero-valent iron (nZVI) [4], iron oxide minerals (goethite, hematite, magnetite and ferrihydrite), iron-immobilized clays [5], and Fe-containing zeolites [6], are used to activate H₂O₂ and generate highly reactive and non-selective •OH. Nevertheless, most of these catalysts show lower catalytic activity than homogeneous Fe²⁺ and need the aid of ultrasound [7,8] and UV/visible light irradiation [9,10], increasing the cost for wastewater treatment.

Recently, iron-copper bimetallic catalyst system has attracted increasing attention [11–13]. For instance, Frank et al. [13] reported iron-copper bimetallic catalyst supported on MCM-41 showed higher catalytic activity than Cu or Fe single supported on MCM-41. In addition, it maintained high catalytic activity even after 10 consecutive runs. Interestingly, similar results were reported on CuFeZSM-5 zeolite [14], Fe-Cu bimetallic oxides supported

* Corresponding author at: Department of Chemistry, Tongji University, 1239 Siping Road, Shanghai 200092, PR China, Tel.: +86 21 65981180; fax: +86 2165982287.
E-mail address: g.zhao@tongji.edu.cn (G. Zhao).

aluminum-containing MCM-41 [12] and mixed Fe, Cu, Al-clays [15]. Our group previously reported magnetic ordered mesoporous copper ferrite (meso-CuFe₂O₄) as a heterogeneous Fenton catalyst for the degradation of imidacloprid [16]. The efficient removal of imidacloprid was achieved and the catalytic activity of meso-CuFe₂O₄ was much higher than nano-Fe₃O₄.

For obtaining a highly catalytic activity of heterogeneous Fenton catalyst, it is necessary for enhancing the dispersity of catalysts and preventing severe aggregation [17]. To achieve these goals, the utilization of porous materials, such as zeolite [5], mesoporous silica [18], active carbon [19], mesoporous carbon and multi-walled carbon nanotubes [20], as supporting materials has been developed. Among them, ordered mesoporous carbon is an interesting material due to its excellent mechanical strength, chemical stability and extraordinary textural characteristics, such as large specific surface area, uniform pore size and accessible mesopores. Generally speaking, for the sake of incorporating heterogeneous catalysts into ordered mesoporous carbon, there are two approaches as follows: (I) impregnating mesoporous carbon into precursor solution, then translating it into required composite catalyst, (II) introducing precursor during the synthesis process of mesoporous carbon, namely “one-pot” synthesis strategy [21,22]. However, the composite catalysts prepared by the impregnation method show poor stability due to the weak interaction force between the catalyst and supporting materials in acid media. In contrast, the composite catalysts fabricated by “one-pot” strategy show excellent stability because of the spatial effect of ordered mesoporous carbon. Moreover, efficient catalytic activity is achieved owing to heterogeneous catalyst highly dispersed in ordered mesoporous carbon. For example, Kong et al. [23] reported a coordinatively unsaturated manganese monoxide-containing mesoporous carbon catalyst which was used in wet peroxide oxidation of phenol. It showed excellent stability, without obvious activity losing or metal leaching after reusing 20 times. Furthermore, the high specific surface area of mesoporous carbon is contributed to the adsorption for organic contaminants in wastewater. Such as, Zhang et al. [24] synthesized mesoporous carbon capsules encapsulated with magnetite nanoparticles, exhibiting higher adsorption capacities and faster adsorption rates of pollutants molecules compared with commercial activated carbon.

In this work, we demonstrated an ordered mesoporous carbon composite catalyst. Iron-copper bimetallic nanoparticles highly dispersed in the matrix of ordered mesoporous carbon. Here, “one-pot” block-copolymer self-assembly strategy and in situ reduction were used to synthesize this composite catalyst. For evaluating its catalytic activity in the heterogeneous Fenton reaction, eight persistent organic compounds were chosen as model contaminants. For comparisons, the monometallic composite catalysts (Fe-MC and Cu-MC) were prepared by the similar method. The main purpose of this study is to elucidate the role of ordered mesoporous carbon and the synergistic effect of iron and copper in the degradation of organic contaminants.

2. Experimental

2.1. Chemicals

Poly(propylene oxide)-block-poly(ethylene oxide)-block-poly(propylene oxide) triblock copolymer Pluronic F127 (PEO₁₀₆PPO₇₀PEO₁₀₆, $M_w = 12,600$) was purchased from Sigma-Aldrich. 5,5-dimethylpyrrolidine-1-oxide (DMPO) was obtained from Aladdin Industrial Corporation. Phenol (C₆H₅OH, 99.98 wt%), formalin solution (HCHO, 37.0–40.0 wt%), sodium hydroxide (NaOH, minimum 96.0%), hydrochloric acid (HCl, 36.0–38.0 wt%), ethanol (C₂H₅OH, minimum 99.7 wt%), iron (III)

nitrate nonahydrate (Fe(NO₃)₃·9H₂O, 98.0 wt%) and copper (II) nitrate trihydrate (Cu(NO₃)₂·3H₂O, 98.0 wt%) were purchased from Shanghai Chemical Corporation. All chemicals were used as received without any further purification. Water used in all synthesis was distilled and deionized.

2.2. Preparation of iron-copper bimetallic composite catalysts

The carbon precursors, soluble Resol Resins, were synthesized from phenol and formaldehyde in a base-catalyzed process [25]. In a typical preparation of composite catalysts, 1.0 g Pluronic F127 was dissolved in 20 g ethanol to form a transparent solution at 35 °C. Then, 0.1010 g Fe(NO₃)₃·9H₂O and 0.0302 g Cu(NO₃)₂·3H₂O (molar ratio 1:2) were added to obtain a dark solution. 5.0 g Resol precursors solution (20 wt%) was added and constantly stirred for 10 min. Subsequently, the mixed solution was poured into multiple dishes to evaporate the ethanol at room temperature for 8 h. Later, the dishes were placed in an oven (100 °C) for 24 h to induce polymerization. Finally, the composites were scraped from the dishes and pyrolyzed at 800 °C for 4 h with a ramping rate of 2 °C/min under nitrogen atmosphere. The obtained composite products were denoted as CuFe-MC-X-T. The X represents the mass of iron precursor (Fe(NO₃)₃·9H₂O) and T represents the calcined temperature. For example, CuFe-MC-1-800 represents that the mass of iron precursor is 0.1010 g and the composite is calcined at 800 °C. While the mass of iron precursor for CuFe-MC-2-800 and CuFe-MC-3-800 are 0.2020 and 0.4040 g, respectively. For the purpose of comparisons, two monometallic composite catalysts, denoted as Cu-MC-1-800 and Fe-MC-1-800, were prepared by the similar method.

2.3. Characterization

TEM images were conducted on a JEM 2100 operated at 200 kV. High resolution scanning electron microscopy (HRSEM) images were obtained on a Hitachi S-4800. XRD patterns were measured on a Bruker D8 Advance X-ray diffractometer using Cu K α ($\lambda = 1.540$ 562 Å, 40 kV, 40 mA) as radiation. N₂ adsorption-desorption isotherms were measured at 77 K with a Micromeritics Tristar3000 analyzer. Before measurement, the samples were degassed in a vacuum at 200 °C for at least 4 h. The metal loadings on ordered mesoporous carbon were determined by inductively coupled plasma-atomic emission spectrometry (ICP-AES, PE OPTIMA 2100DV). ESR spectra were obtained on a Bruker EMX X^{plus}-10/12 with Microwave Bridge (microwave frequency, 9.853 GHz; microwave power, 20 mW; modulation amplitude, 1 G; modulation frequency, 100 kHz). For ESR measurement, 25 μ L of the sample was collected from the suspension system and immediately mixed with 25 μ L of 0.22 M DMPO to form DMPO·OH adduct.

2.4. Degradation experiments of BPA and sample analysis

Batch degradation experiments of BPA were carried out in a cylindrical reactor with a double jacket for circulation of external thermostatic water to regulate the solution temperature. Before the reaction, all the catalysts were dried in the vacuum drying oven at 120 °C for 2 h. In a standard experiment, 30 mg catalyst was mixed with 100 mL of BPA (100 mg L⁻¹). The suspension was vigorously stirring for 60 min to achieve the adsorption/desorption equilibrium between BPA molecular and catalyst. Then, 300 μ L H₂O₂ (30 wt%) was added into the suspension. The initial pH was adjusted to the required pH by using 0.1 M H₂SO₄. Samples were taken at 10 min intervals using a 5 mL syringe, filtered immediately through a 0.22 μ m filter film and analyzed by HPLC with a Varian Prostar 310 system equipped with Varian AQ-C18 column (4.6 mm \times 150 mm \times 5 μ m). The mobile phase was a mixture of methanol and water (70:30, v/v) with a flow rate of 1.0 mL min⁻¹,

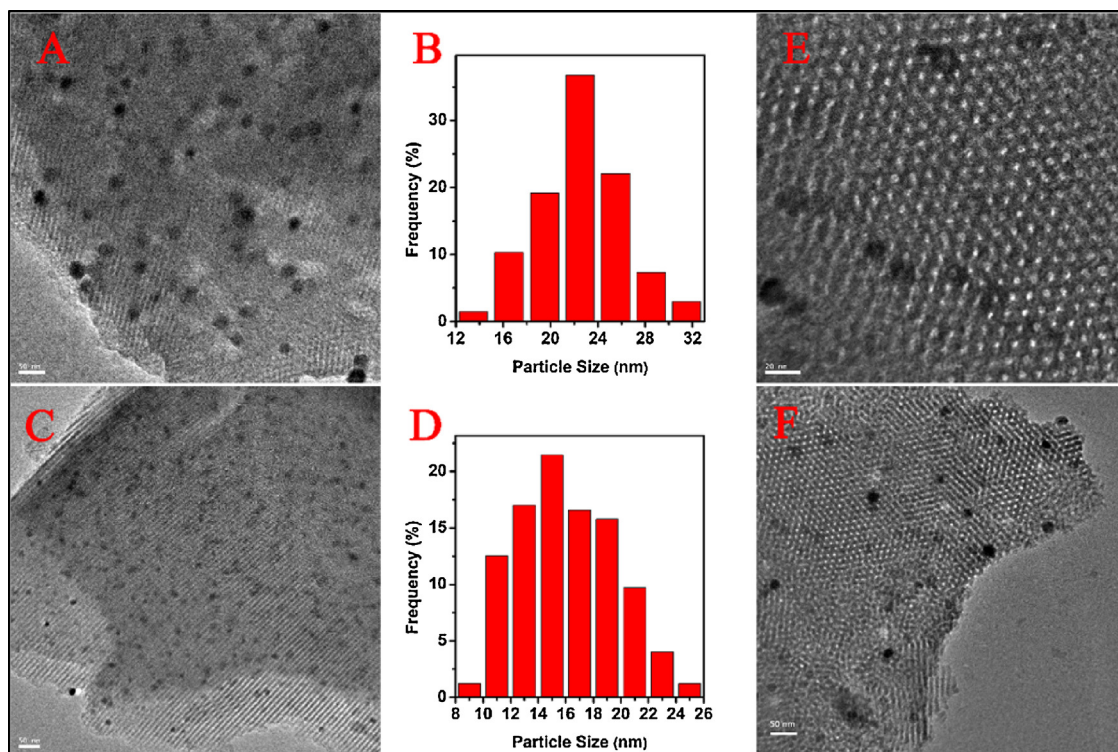


Fig. 1. TEM images of CuFe-MC-1-800 (A and E) and Fe-MC-1-800 (C and F) viewed along the [110] (A and C), and [001] (E and F) directions, respectively. The middle (B and D) are the metal nanoparticle size distribution histogram calculated from A and C, respectively.

the injection volume was 20 μL , and the UV detector was operated at 225 nm. The quantitation of $\bullet\text{OH}$ was determined with the method which was reported in the previous literature [26]. The concentration of iron leaching was measured with 1,10-phenanthroline method by recording the absorbance at 510 nm. The samples were measured using an Agilent 8453 UV-vis spectrophotometer with a 1 cm path length spectrometric quartz cell. TOC values were determined by a Multi 3100 TOC/TN analyzer. For TOC analysis, all the samples were immediately treated with scavenging reagent (0.1 M Na_2SO_3 , 0.1 M KH_2PO_4 , 0.1 M KI and 0.05 M NaOH) to obtain accurate TOC value [27]. The scavenging reagent acts as reduction and precipitation agent. This procedure led to a complete reduction of the residual H_2O_2 as well as to the removal of most of the $\text{Fe}^{2+}/\text{Fe}^{3+}$ [28,29].

3. Results and Discussion

3.1. Morphology and physicochemical properties of catalysts

TEM images of CuFe-MC-1-800 (Fig. 1A and E) and Fe-MC-1-800 (Fig. 1C and F) show stripe-like and hexagonally arranged patterns in large domains, confirming an ordered 2D hexagonal mesostructure. Fig. 1A and C are viewed along the [110] direction, and Fig. 1E and F are viewed along the [001] direction. The mean pore sizes of CuFe-MC-1-800 and Fe-MC-1-800 are approximate 4.3 and 4.2 nm, respectively. The dark spots are observed for CuFe bimetallic nanoparticles, which are highly dispersed in the matrix of ordered mesoporous carbon. Fig. 1B and D shows the particle size distribution histogram of bimetallic nanoparticles. The average sizes of nanoparticles in CuFe-MC-1-800 and Fe-MC-1-800 are approximate 17 and 16 nm, respectively. HRSEM images of CuFe-MC-1-800 and Fe-MC-1-800 are shown in Fig. 2. They show oriented and hexagonally arranged pores, confirming highly ordered 2D hexagonal mesostructure, which are consistent with TEM results. SEM can give an elemental distribution map through

Table 1

The EDS results of the catalyst of CuFe-MC-1-800.

Element	Mass ratio	Atomic ratio
C K	93.46	95.90
O K	4.80	3.70
Na K	0.11	0.06
Fe K	1.08	0.24
Cu K	0.55	0.11
Total	100.00	100.00

images of back-scattered electron and EDS as well as surface topographic information through those of secondary electrons [30]. Fig. 3 shows SEM photograph and the corresponding EDS elemental mapping of CuFe-MC-1-800. The EDS elemental maps confirm that C, O, Cu and Fe elements are highly dispersed in CuFe-MC-1-800. The relative atomic content of these element are listed in Table 1, and the atomic ratio of copper and iron is 0.46, approximate to the theoretical value, 1:2.

Wide-angle X-ray diffraction (WAXRD) patterns of iron-copper bimetallic composite catalysts calcined at different temperature are shown in Fig. 4. The catalyst calcined at 400 $^{\circ}\text{C}$ shows three diffraction peaks centered at $2\theta \approx 43.2^{\circ}$, 50.4° and 74.1° , corresponding to the (111), (200) and (220) reflections of copper (JCPDS Card No. 99-0034). When the calcined temperature increases to 600 $^{\circ}\text{C}$, another four diffraction peaks appear at 31.5° , 35.3° , 44.6° and 64.9° . Among them, the diffraction peak at 31.5° maybe contributes to CuFeO_2 , 35.3° contributes to Fe_3C , and 44.6° and 64.9° contribute to iron (JCPDS Card No. 87-0721) which is formed by in situ reduction during the calcination. And the size of iron nanoparticles is calculated to be about 28 nm by Scherrer equation. When the calcined temperature increases to 800 $^{\circ}\text{C}$, the diffraction peak at 31.5° disappears, suggesting iron oxide be completely reduced. For the purpose of comparisons, two monometallic composite catalysts (Fe-MC and Cu-MC) were prepared by the similar method.

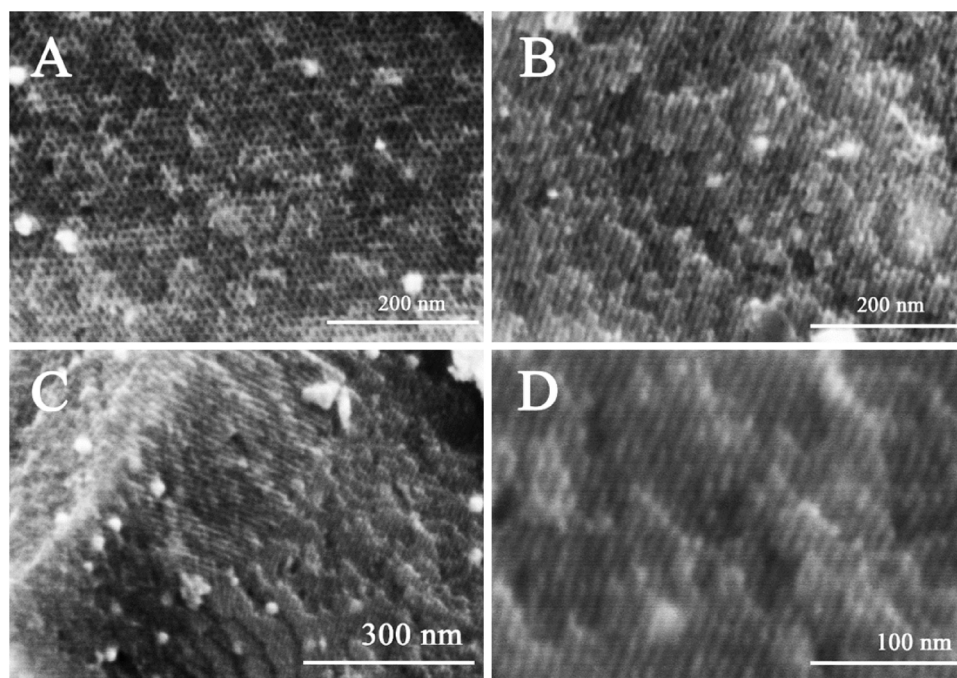


Fig. 2. HRSEM images for CuFe-MC-1-800 (A and B) and Fe-MC-1-800 (C and D).

As shown in Fig. 4a, five diffraction peaks centered at $2\theta \approx 30.1^\circ$, 35.5° , 43.1° , 57.3° , 62.7° are observed about Fe-MC-1-800, which can be assigned to 2 2 0, 3 1 1, 4 0 0, 5 1 1 and 4 4 0 reflections of γ - Fe_2O_3 (JCPDS Card No. 89-5892). Three diffraction peaks centered at $2\theta \approx 43.2^\circ$, 50.4° and 74.1° are observed about Cu-MC-1-800, and the size of copper nanoparticles is calculated to be about 29 nm. It can be concluded that iron nanoparticles do not formed without the doping of copper, possibly due to the interaction between iron and copper decreases the reduction temperature of iron.

N_2 adsorption-desorption isotherms of composite catalysts show representative type-IV curves with H1 hysteresis loops (Fig. 5). Nitrogen filling occurs approximately at $P/P_0 = 0.40$ – 0.80 owing to the capillary condensation, reflecting a high uniformity of mesopore sizes. The pore size distribution curves calculated from desorption branches clearly confirm their narrow pore size distribution. The BET surface area of ordered mesoporous carbon (MC-800) is $573 \text{ m}^2 \text{ g}^{-1}$. Interestingly, when iron and copper doped into ordered mesoporous carbon, the BET surface areas of Cu-MC-1-800, Fe-MC-1-800 and CuFe-MC-1-800 are 626, 619 and $639 \text{ m}^2 \text{ g}^{-1}$, respectively (Table 2). The mean pore sizes of MC-800, Cu-MC-1-800, Fe-MC-1-800 and CuFe-MC-1-800 are 2.2, 3.6, 3.6 and 3.8 nm, respectively (Table 2). This phenomenon confirms that metal doped into ordered mesoporous carbon contributes to increase BET surface area and pore size of mesoporous carbon. The reason is that iron and copper entrapped into ordered mesoporous carbon can hinder the shrinkage of carbon matrix during the carbonization process. Besides, the influence of mesostructure by calcined temperature was studied. The results show that calcined temperature remarkably affected the mesostructure of composites. The BET surface areas of CuFe-MC-1-400 and CuFe-MC-1-600 are 466 and $666 \text{ m}^2 \text{ g}^{-1}$, respectively. This is attributed to that F127 and Resol molecules are partially carbonized at 400°C , while almost completely carbonized at 600°C . Nevertheless, when the calcined temperature increase to 800°C , the BET surface area reduce slightly since the matrix of ordered mesoporous carbon occur shrinkage. These results are in well agreement with the SAXRD data. In addition, when the contents of iron and copper increase, the BET surface

areas of CuFe-MC-2-800 and CuFe-MC-3-800 reduce to 551 and $510 \text{ m}^2 \text{ g}^{-1}$, respectively.

Small-angle X-ray diffraction (SAXRD) patterns of composite catalysts with same Fe contents (2.3 wt%) calcined at different temperature are shown in Fig. 6. They show typical low-angle reflections characteristic of the 2D hexagonal mesostructure (space group $p6mm$), which with one strong line and one weak line attributable to the (10) and (11) reflections. SAXRD pattern of CuFe-MC-1-400 shows an obvious diffraction peak at 0.76° . With the calcined temperature increased to 600 and 800°C , the diffraction peaks shift to 0.82° and 0.88° , respectively. For CuFe-MC-1-400, CuFe-MC-1-600 and CuFe-MC-1-800, the unit-cell parameters (a_0) calculated from the formula $a_0 = 2d_{10}/\sqrt{3}$ are 13.4, 12.4 and 11.6 nm, respectively. The average pore sizes calculated by BJH method are 3.9, 3.6 and 3.8 nm, respectively. Therefore, the pore wall thicknesses calculated from the formula $h = a_0 - D_p$ are 9.5, 8.8 and 7.8 nm, respectively. This phenomenon indicated that the matrix of mesoporous carbon shrink and the pore wall thickness decrease as the calcined temperature increasing. It should be mentioned that a_0 value of CuFe-MC is larger than that of mesoporous carbon (10.0 nm). This result indicates the introduction of iron and copper into polymer framework may remarkably inhibit its shrinkage during the calcination process. This phenomenon is consistent with what is observed when inorganic silica nanoparticles are present in the mesoporous carbon framework [31]. Another phenomenon should be noticed is that the intensity of diffraction peaks of composites decreases as the amount of iron percent increasing. For instance, the featured diffractions of CuFe-MC-3-800 in small-angle range are very weak. These observations indicate that some nanoparticles are located inside mesoporous carbon pores while some are located at the orifice of pores. Obviously, moderate iron content is favorable to the ordered mesostructure of composite catalysts.

3.2. TOC removal and BPA degradation

The performance of the as-prepared composite catalysts were estimated by degrading various recalcitrant organic contaminants.

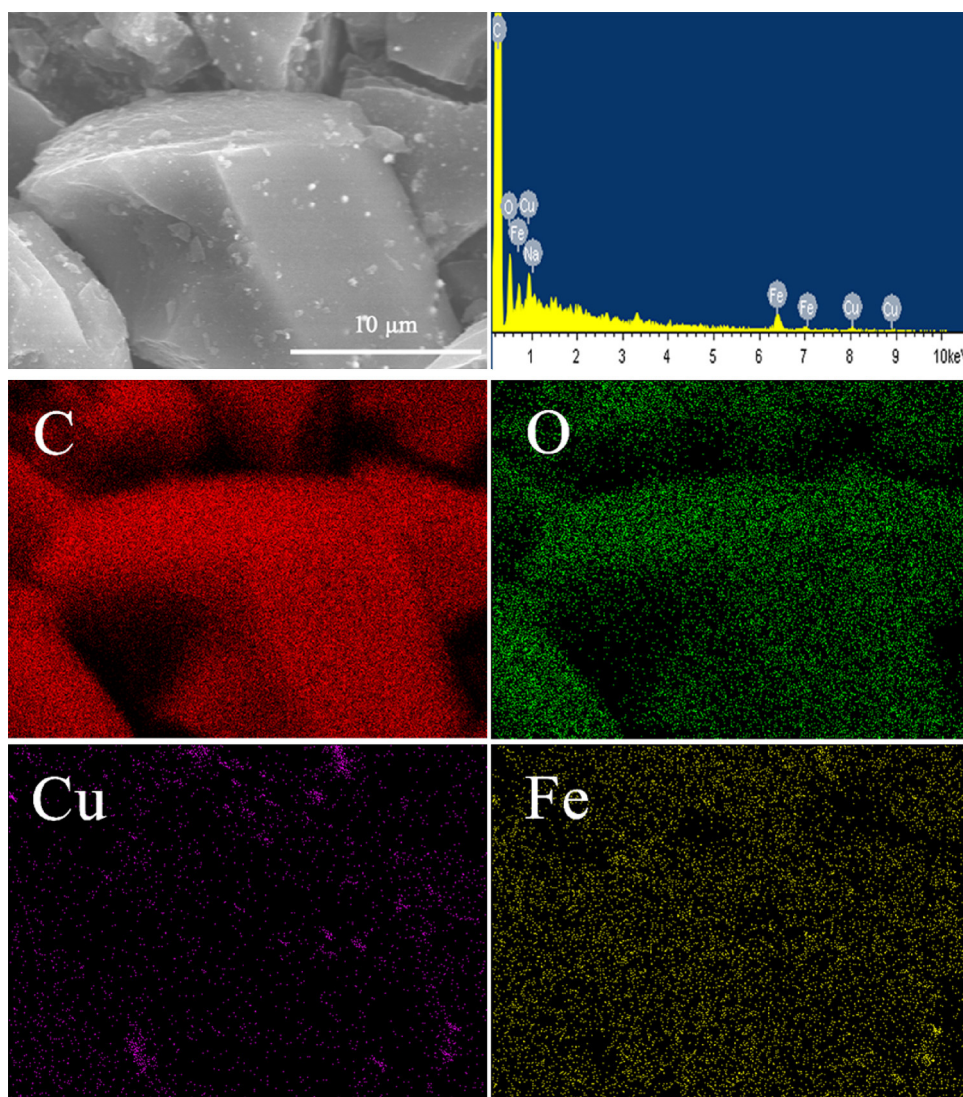


Fig. 3. SEM photograph and elemental mapping images of CuFe-MC-1-800 for C, O, Cu and Fe with color superposition (C = red; O = green; Cu = purple; and Fe = yellow). (For interpretation of the references to color in this figure legend, the reader is referred to the web version of the article.)

Eight organic compounds were chosen as model contaminants. Phenol, widely used as industrial materials or intermediates, is one of the most toxic organics discharged by many manufactories [32]. Benzoic acid is a common contaminant in the wastewater from coal chemical plant [33]. Bisphenol A, regarded as a potential

endocrine-disruptor, has been detected in food, water, paper and plastic products [34]. 2,4,6-Trichlorophenol is a chlorinated organic contaminant and has a stable aromatic structure. Imidacloprid (IMI) is one of the insecticides most used in agricultural areas [35]. Ketoprofen is recognized as a refractory and hazardous component

Table 2
Textural properties of ordered mesoporous carbon nanocomposites.

Sample	Fe content ^a [wt%]	Cu content ^a [wt%]	S_{BET} [m ² g ⁻¹]	V_t [cm ³ g ⁻¹]	a_0 [nm]	D_p [nm]	h [nm]	Particle size ^c [nm]	Particle size ^d [nm]
CuFe-MC-1-400	<i>b</i>	<i>b</i>	466	0.50	13.4	3.9	9.5	–	–
CuFe-MC-1-600	<i>b</i>	<i>b</i>	666	0.59	12.4	3.6	8.8	–	–
CuFe-MC-1-800	2.3	1.2	639	0.56	11.6	3.8	7.8	26	17
CuFe-MC-2-800	4.5	2.7	551	0.49	13.1	3.8	9.3	–	–
CuFe-MC-3-800	7.5	4.7	510	0.43	–	3.6	–	–	–
Fe-MC-1-800	1.5	0.0	619	0.45	11.6	3.6	8.0	25	16
Cu-MC-1-800	0.0	2.0	626	0.50	–	3.6	–	–	–
MC-800	0.0	0.0	573	0.33	10.0	2.2	7.8	–	–

The d -spacing values were calculated according to the formula $d = 0.15408 / 2 \sin \theta$, and the unit-cell parameters were calculated from the formula $a_0 = 2d_{10}/\sqrt{3}$, the pore wall thickness were calculated from the formula of $h = a_0 - D_p$. The pore size distributions were derived from the desorption branches of isotherms.

^a Estimated from ICP-AES analysis.

^b Not detected.

^c Calculated by Scherrer equation.

^d Calculated by TEM.

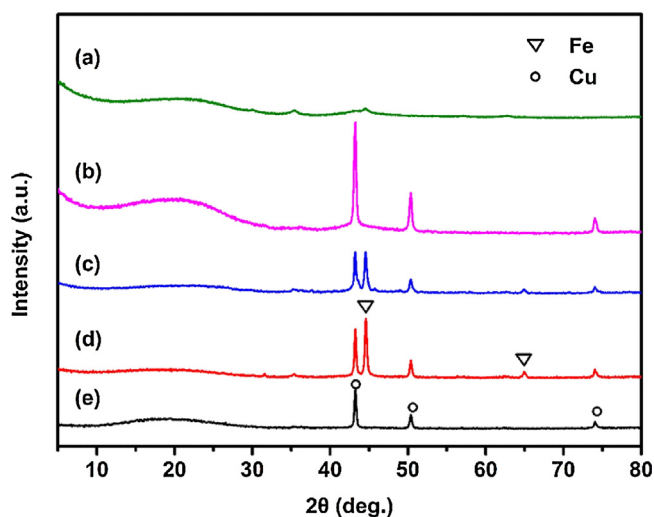


Fig. 4. XRD patterns of different catalysts: (a) Fe-MC-1-800, (b) Cu-MC-1-800, (c) CuFe-MC-1-800, (d) CuFe-MC-1-600 and (e) CuFe-MC-1-400.

in pharmaceutical wastewater [36]. Methylene blue and methyl orange are extensively used in textile industry. TOC removal was measured to evaluate the mineralization of organic contaminants. As listed in Table 3, higher than 80% TOC removal of most contaminants (initial 100 mg L^{-1}) are achieved in 12 h, indicating high catalytic activity of CuFe-MC for the mineralization of various organic contaminants. As we known, homogeneous Fenton reagent is powerful for the degradation of organic compounds. For the purpose of comparison, comparable amount Fenton reagent is used for mineralization of organic contaminants. The mineralization results suggest that the TOC removal in the system of CuFe-MC- H_2O_2 is all higher than Fe^{2+} - H_2O_2 system. For example, about 94% of TOC removal is observed in the system of CuFe-MC- H_2O_2 -IMI after 12 h reaction, while only 38% in Fe^{2+} - H_2O_2 -IMI system.

In order to further investigate the catalytic activity of CuFe-MC, BPA was selected as a model contaminant. The degradation of BPA catalyzed by different catalysts was evaluated. Before H_2O_2 added, the suspension was continuously stirring for 60 min to achieve the adsorption/desorption equilibrium between BPA molecular and catalysts. As shown in Fig. 7a, the removal of BPA by adsorption is 42% with CuFe-MC-1-800 as catalyst, confirming its favorable adsorption property. The good adsorption property of CuFe-MC-1-800 is related to its high BET surface area ($639 \text{ m}^2 \text{ g}^{-1}$) and large pore size (3.8 nm). It is observed that within 60 min the concentration of BPA diminishes very slowly with only H_2O_2 added, which is ascribed to the weak oxidation potential of H_2O_2 compared with $\bullet\text{OH}$. However, rapid degradation of BPA is achieved 93% catalyzed by CuFe-MC-1-800 with 300 mg L^{-1} catalyst dosage, indicating the high catalytic ability for H_2O_2 activation. In contrast, the

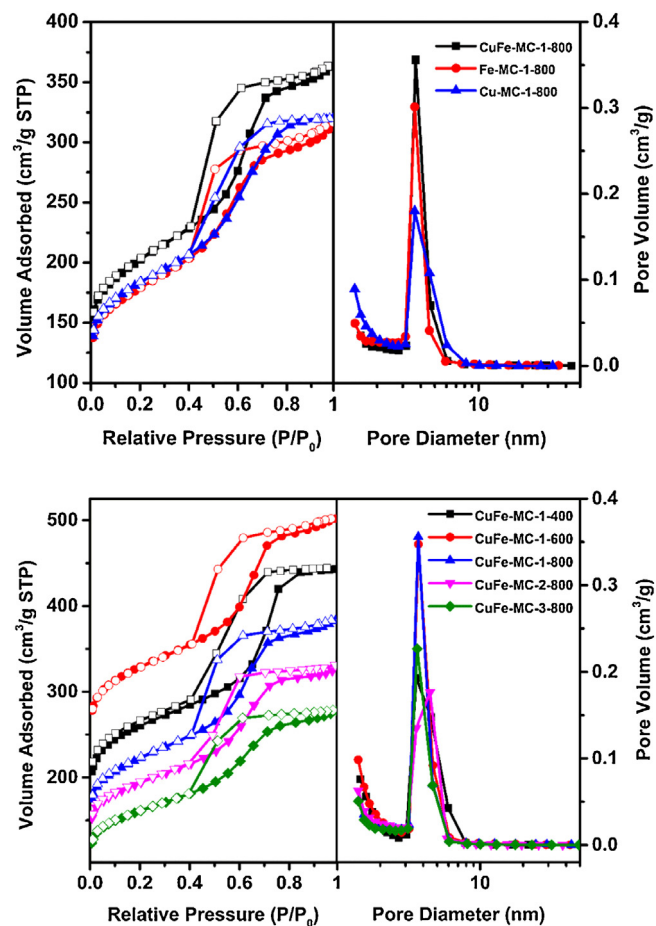


Fig. 5. Nitrogen sorption isotherms (left) of nanocomposites catalysts and the corresponding pore size distribution curves (right) calculated from desorption branches via the Barrett-Joyner-Halenda (BJH) method. The isotherm of CuFe-MC-1-800 and CuFe-MC-2-800 are offset vertically by $20 \text{ cm}^3 \text{ g}^{-1}$ and the isotherm of CuFe-MC-1-400 and CuFe-MC-1-600 are offset vertically by $120 \text{ cm}^3 \text{ g}^{-1}$.

degradation ratios of BPA by Fe-MC-1-800 and Cu-MC-1-800 are 64% and 40%, respectively. The removal of BPA by Cu-MC-1-800 is almost owing to adsorption, and the catalysis could be ignored. Therefore, the efficient removal of BPA by CuFe-MC-1-800 is not only due to its good adsorption property, but also the synergistic effect of iron and copper entrapped in the matrix of ordered mesoporous carbon. The highly dispersed of Fe, Cu nanoparticles effectively increase the number of active sites, leading to the efficient catalytic activity for the activation of H_2O_2 . Similar catalysts reported by other groups also show enhancing catalytic activity due to their mesostructure. For example, a core/shell structure

Table 3

Degradation of various robust organic contaminants.

Entry	Contaminants	Initial conc. (ppm)	TOC removal ^a (%)	TOC removal ^b (%)
1	Phenol	100	83.7	73.3
2	Benzoic acid	100	81.4	49.7
3	Bisphenol A	100	66.3	49.8
4	2,4,6-Trichlorophenol	100	93.5	37.6
5	Imidacloprid	100	94.3	38.0
6	Ketoprofen	100	77.8	41.9
7	Methylene blue	100	95.4	55.7
8	Methyl orange	100	86.9	37.3

Reaction conditions: initial $[\text{H}_2\text{O}_2] = 30 \text{ mM}$, 298 K, pH 3.0, 300 mg/L of catalyst.

^a Catalyzed by CuFe-MC-1-800 for 12 h.

^b Catalyzed by homogeneous Fenton ($\text{FeSO}_4 \cdot 7\text{H}_2\text{O}$) for 12 h.

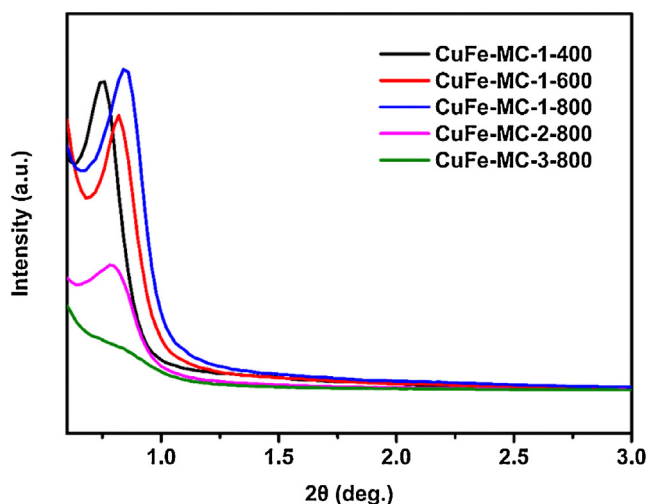


Fig. 6. Small-angle XRD patterns of iron-copper bimetallic composite catalysts. (CuFe-MC-1-400: black; CuFe-MC-1-600: red; CuFe-MC-1-800: blue; CuFe-MC-2-800: magenta; CuFe-MC-3-800: olive.) (For interpretation of the references to color in this figure legend, the reader is referred to the web version of the article.)

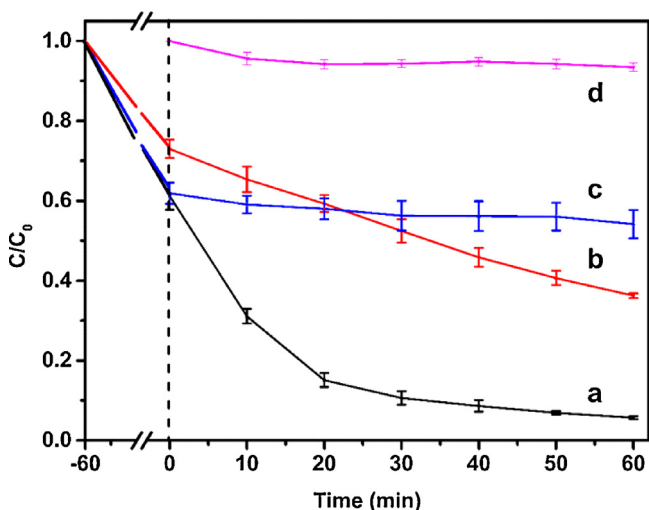


Fig. 7. The degradation of 100 mg L⁻¹ BPA at the initial pH 3.0, 30 mM H₂O₂, catalyst dosage 300 mg L⁻¹ and 25 °C catalyzed by different catalyst: (a) CuFe-MC-1-800; (b) Fe-MC-1-800; (c) Cu-MC-1-800; (d) only H₂O₂, without catalyst addition.

catalyst with CoFe₂O₄ nanoparticles as core and mesoporous carbon capsule as shell exhibits very high catalytic activity for the decomposition of H₂O₂ [17]. MnOx-containing mesoporous carbon catalyst shows high catalytic activity in wet oxidation of phenol and stability [23]. In short, mesoporous carbon play a major role in the adsorption of organic contaminants and subsequent reaction on the surface with active sites. Besides, the large pore size of mesoporous carbon (about 4 nm) could reduce the resistant of mass transfer of reactants and products, resulting in remarkably enhanced performance.

Moreover, the data for BPA concentration decay were further analyzed by kinetic equation. The kinetic equation may be expressed as

$$\ln \left(\frac{C_0}{C} \right) = kt$$

where k is the apparent reaction constant, C_0 and C are the initial concentration and the concentration at time t , of BPA, respectively. The kinetic analysis shows that the degradation of BPA follows the pseudo-first order (see Fig. 8). The apparent rate constants for

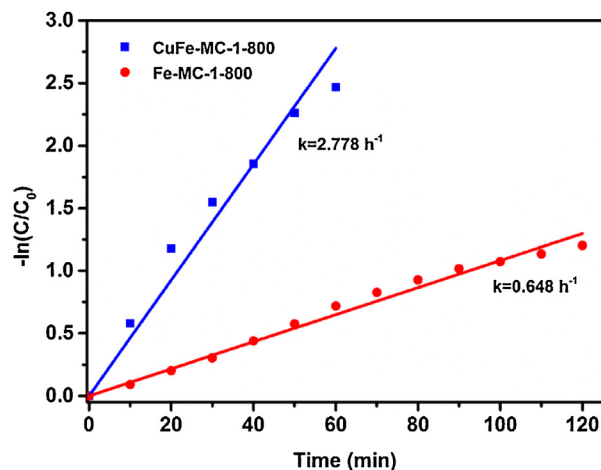


Fig. 8. The kinetic analysis of BPA degradation, that is the dependence of $-\ln(C/C_0)$ versus time.

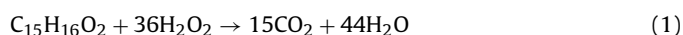
CuFe-MC-1-800 and Fe-MC-1-800 are 2.778 and 0.648 h⁻¹, respectively. The degradation rate of BPA by CuFe-MC-1-800 is about 4 times than Fe-MC-1-800.

The influence of calcined temperature on catalytic activity of CuFe-MC was studied. As seen in Fig. 9A, the degradation ratios of BPA catalyzed by CuFe-MC-1-400, CuFe-MC-1-600 and CuFe-MC-1-800 are 86%, 93% and 93% in 60 min, respectively. However, the degradation rate of BPA by CuFe-MC-1-800 is relatively faster than CuFe-MC-1-400 and CuFe-MC-1-600. Therefore, CuFe-MC-1-800 is chosen as catalyst for the degradation of BPA in the following discussion.

The degradation of BPA was influenced by initial parameters, e.g. catalyst dosage, pH and H₂O₂ concentration. The degradation of BPA along time under different experimental conditions was evaluated. Fig. 9B shows the degradation of BPA by CuFe-MC-1-800 at different catalyst dosage. It can be observed that the removal of BPA by adsorption is enhanced with the catalyst dosage increasing. For instance, the removal of BPA by adsorption achieves 66% when the catalyst dosage is 500 mg L⁻¹. CuFe-MC-1-800 shows excellent adsorption capability for BPA, owing to its high BET surface area and large pore size. The degradation of BPA achieves 85% with 200 mg L⁻¹ catalyst dosage, and up to 91%, 93% and 94% when the catalyst dosages increase to 300, 400 and 500 mg L⁻¹, respectively. The increasing catalyst dosage leads to more BPA molecules adsorbed on the surface of catalyst and more reaction sites contacted to BPA.

The influence of pH on the degradation of BPA by using CuFe-MC-1-800 as catalyst was evaluated. The experiments of degradation of BPA at different pH value, 3.0, 5.0, 7.0 and 9.0, were conducted. The results showed that 93% removal of BPA could be achieved at pH 3.0, and about 58% removal of BPA at pH 5.0 to 9.0. These results indicated that pH had some influence on the degradation of BPA with CuFe-MC-1-800 as catalyst. However, CuFe-MC-1-800 still showed some catalytic activity at higher pH value. This phenomenon maybe related to the valence state of iron-copper and the microenvironment of the surface of CuFe-MC-1-800 [3].

The effect of initial H₂O₂ concentration on the catalytic activity of CuFe-MC-1-800 was also investigated. According to Eq. (1), the theoretical H₂O₂ stoichiometric molar ratio for total mineralization of BPA is 36. Therefore, 15.8 mM H₂O₂ is required for complete mineralization of 100 mg L⁻¹ BPA.



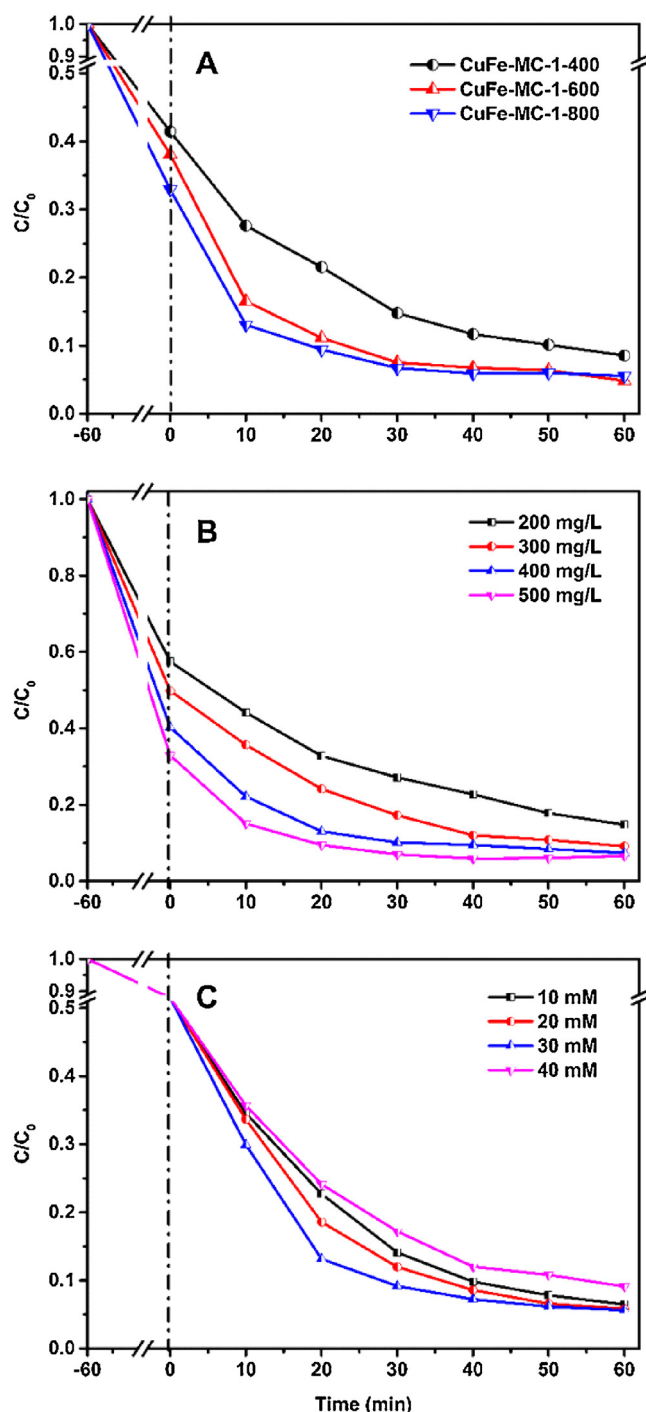


Fig. 9. The degradation of BPA in the Fenton process catalyzed by CuFe-MC: (A) catalysts prepared at different temperature (400, 600 and 800 °C); (B) catalyst dosage; (C) H_2O_2 initial concentration. Except for the investigated parameter, other parameters fixed on pH 3.0, H_2O_2 30 mM, CuFe-MC-1-800 300 mg L^{-1} , BPA 100 mg L^{-1} and temperature 25 °C.

In the experiment process, 10, 20, 30 and 40 mM H_2O_2 were chosen. As shown in Fig. 9C, the degradation of BPA is gradually accelerated with H_2O_2 concentration increasing from 10 to 30 mM. The reason for this is that 10 mM less than the theoretical amount of H_2O_2 for complete mineralization of 100 mg L^{-1} BPA. However, the degradation rate of BPA remarkably decreases when 40 mM H_2O_2 is used. This is probably due to unprofitable consumption of H_2O_2 from the scavenging effect of H_2O_2 , which may be described by Eqs.

(2) and (3) [37]. Based on the above analysis, 30 mM H_2O_2 is chosen as the optimal initial concentration in the degradation of BPA.



3.3. Identification of intermediates, possible degradation pathways and toxicity

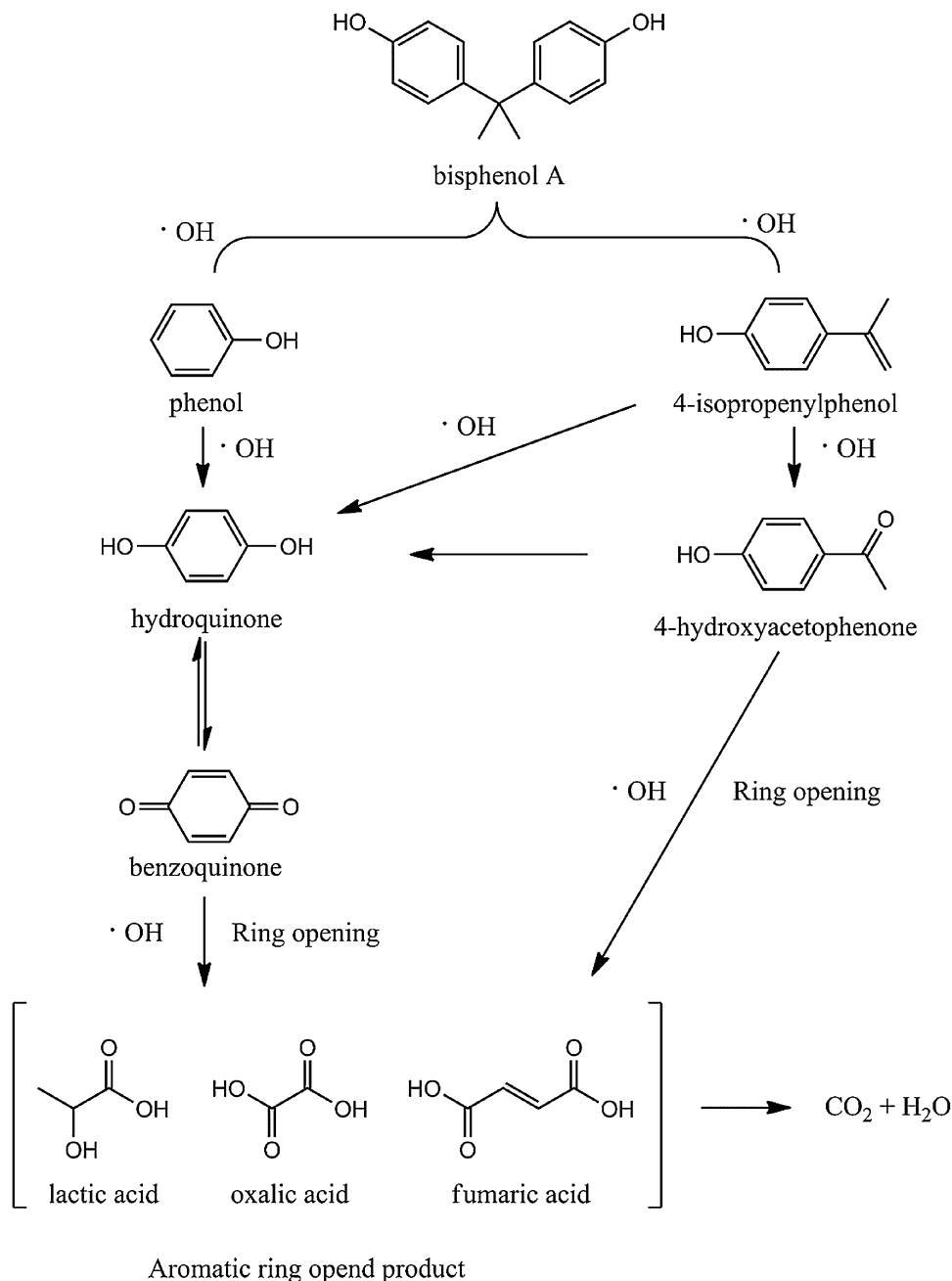
The intermediates formed during the heterogeneous Fenton oxidation of BPA over CuFe-MC-1-800 catalyst were identified by HPLC and GC–MS analysis. Five compounds, 4-isopropenylphenol, hydroquinone, 4-hydroxyacetophenone, benzoquinone and phenol, were identified in the work. Based on the present experimental data and the previous literatures [38–40], the possible degradation pathways of BPA were proposed in Scheme 1. The $\bullet\text{OH}$ played the major role in the heterogeneous Fenton oxidation of BPA. In the primary degradation of BPA, the $\bullet\text{OH}$ attacked the electron-rich C2 of BPA to generate 4-isopropenylphenol and phenol, which was further translated into hydroquinone. These aromatic intermediates could be sequentially oxidized through ring opening reaction to yield aliphatic compounds such as lactic, oxalic acid and formic acid, and finally mineralized into CO_2 and H_2O .

It should be emphasized that the intermediates formed within 12 h maybe more toxic than BPA. The identified intermediates included hydroquinone (LD50: 245 mg kg^{-1} ; oral dose, mouse), 4-hydroxyacetophenone (1500 mg kg^{-1}), benzoquinone (25 mg kg^{-1}) and phenol (270 mg kg^{-1}), which were all more toxic than BPA (2400 mg kg^{-1}) [41]. However, 66.3% TOC removal of BPA was achieved after 12 h. Besides, the relative concentration variety of intermediates were investigated. 4-Hydroxyacetophenone and phenol could be completely decomposed in 2 h. The concentration of hydroquinone and benzoquinone achieved maximum in 10 min and then diminished. And the concentration of small molecular acid, such as lactic, oxalic acid and formic acid, achieved maximum in 40 min and then reduced slowly. The results showed that these high toxic intermediates could be decomposed through further structure fragmentation and mineralization, finally resulting in the nontoxic products to freshwater species. Similar result was reported by other group [42].

3.4. Plausible mechanism

To ascertain the reaction mechanism, 5,5-dimethylpyrroline-1-oxide (DMPO) spin-trap ESR was performed to examine $\bullet\text{OH}$ produced in the heterogeneous Fenton reaction. For bare ordered mesoporous carbon (a curve of Fig. 10d), the signal of DMPO- $\bullet\text{OH}$ adduct is very weak, suggesting low catalytic activity of ordered mesoporous carbon for the activation of H_2O_2 . However, other three ESR spectra exhibit a 4-fold characteristic peaks of DMPO- $\bullet\text{OH}$ adducts with an intensity ratio of 1:2:2:1. The results clearly indicate that all of three catalysts could active H_2O_2 to generate $\bullet\text{OH}$. And the intensity of peak of DMPO- $\bullet\text{OH}$ adducts by using CuFe-MC as catalyst is much higher than Fe-MC and Cu-MC, demonstrating the higher catalytic activity of CuFe-MC.

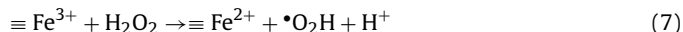
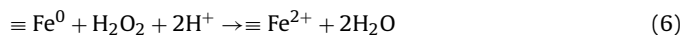
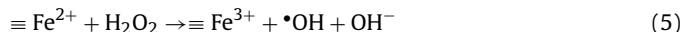
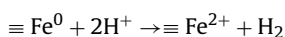
As we known, it is difficulty that quantitatively determine the concentrations of $\bullet\text{OH}$ by ESR spectra. In order to quantitatively determine the cumulative amount of $\bullet\text{OH}$, HPLC was performed by using benzoic acid as a probe molecular. The reaction rate constant of benzoic acid reacting with $\bullet\text{OH}$ in aqueous media is $4.2 \times 10^9 \text{ M}^{-1} \text{ s}^{-1}$. It is reported that per mole *p*-HBA is produced quantitatively by $5.87 \pm 0.18 \text{ mol } \bullet\text{OH}$ [26]. The obtained results were displayed in Fig. 11. For instance, the amount of $\bullet\text{OH}$ generated by CuFe-MC-1-800 within 60 min is up to 325 μM , which is approximate ten times higher than the heterogeneous Fenton catalyst of meso-CuFe₂O₄ (32.9 μM) previously reported by our group [16].



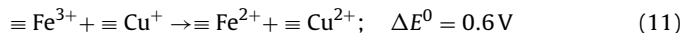
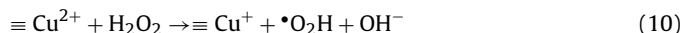
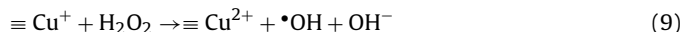
Scheme 1. Possible pathways of BPA degradation induced by $\cdot\text{OH}$ radicals in the CuFe-MC-1-800/ H_2O_2 system.

And the amount of $\cdot\text{OH}$ generated by Fe-MC-1-800 and Cu-MC-1-800 are 112 and 55 μM , respectively. $\cdot\text{OH}$ as a major oxidizing species plays an important role in heterogeneous Fenton process. Therefore, it may be the reason that organic contaminants could be rapidly degraded by CuFe-MC-1-800.

Plausible mechanism was proposed based on the results of XRD and ESR spectra. The heterogeneous Fenton reaction catalyzed by CuFe-MC-1-800 proceeds via surface reaction involving both Cu and Fe active sites as given below. In the initial step, zero valent iron is oxidized to Fe^{2+} via a two electron transfer from the nanoparticle surface to H_2O_2 (Eqs. (4) and (6)) [4,43]. Then, Fe^{2+} active H_2O_2 to generate $\cdot\text{OH}$ according to Haber–Weiss mechanism (Eq. (5)). Simultaneously, the regeneration of Fe^{2+} from Fe^{3+} could be achieved through Eq. (8).



Similar with Fe^{2+} , Cu^+ also can active H_2O_2 decomposition to generate $\cdot\text{OH}$. The reaction equations are presented as follows [44]:



Since the standard reduction potential of $\text{Fe}^{3+}/\text{Fe}^{2+}$ is 0.77V and $\text{Cu}^{2+}/\text{Cu}^+$ is 0.17V, thus the reduction of Fe^{3+} by Cu^+ (Eq.

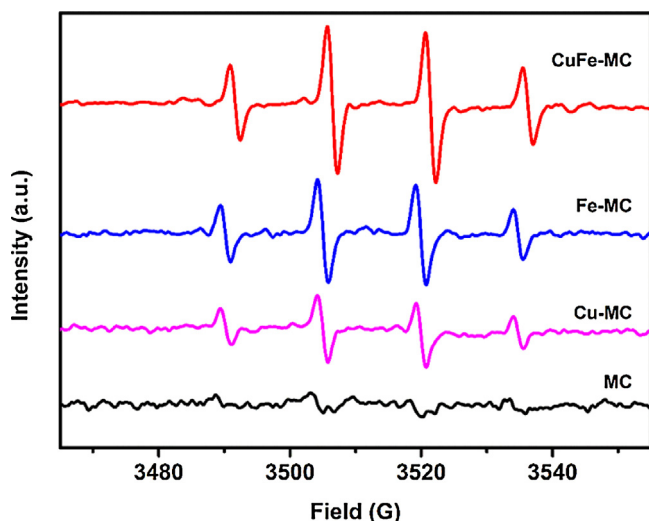


Fig. 10. DMPO spin trapping ESR spectra of hydroxyl radicals.

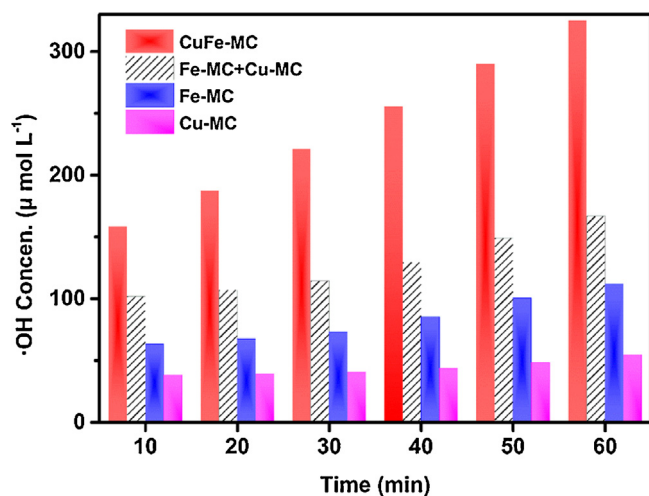


Fig. 11. The concentrations of $\cdot\text{OH}$ generated as a function of time for 300 mg L^{-1} catalyst dosage, $30\text{ mM H}_2\text{O}_2$, and pH 3.00 at 25°C . Benzoic acid used as a probe at 10 mM .

(11) is thermodynamically favorable, which is benefit for the redox cycles of $\text{Fe}^{3+}/\text{Fe}^{2+}$ and $\text{Cu}^{2+}/\text{Cu}^+$. Therefore, by the role of both $\text{Fe}^{3+}/\text{Fe}^{2+}$ and $\text{Cu}^+/\text{Cu}^{2+}$ pair, the interfacial electron transfer is greatly enhanced in CuFe-MC-1-800. Therefore, thanks to the

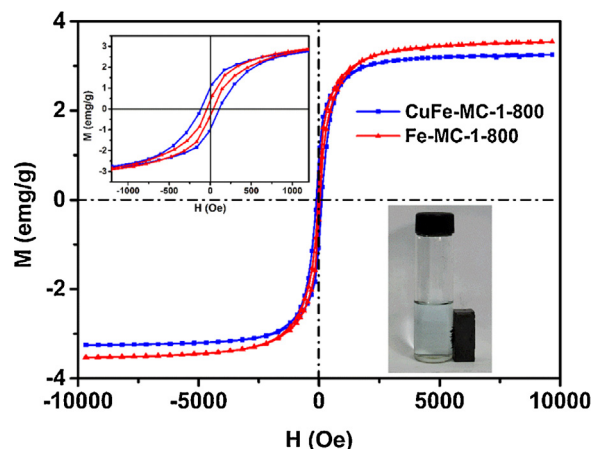


Fig. 13. Magnetization curves of CuFe-MC-1-800 and Fe-MC-1-800 composite catalysts and optical photo (inset) of the samples in the ethanol solution separated by a magnet.

synergistic effect of iron and copper entrapped in the matrix of ordered mesoporous carbon, CuFe-MC presents the best catalytic activity for the degradation of organic contaminants.

3.5. The stability and recyclability of catalysts

Cycling instability is a persisting problem in heterogeneous Fenton catalysis. From the view of actual application, the long-term stability of CuFe-MC is very significant. Therefore, the leaching characteristic and the activity variation of CuFe-MC in cycles are especially concerned. Therefore, the leaching iron was measured with 1,10-phenanthroline method. The concentration of total dissolved iron is 0.57 mg L^{-1} after 60 min reaction, much lower than 2 mg L^{-1} which is the legal limit imposed by the directives of the European Union [18]. This phenomenon confirms that the stability of composite catalysts is enhanced due to the confinement effect of ordered mesoporous carbon. Successive experiments were performed to evaluate the possibility of CuFe-MC reuse. As shown in Fig. 12, it is observed that CuFe-MC-1-800 remains high catalytic activity after five consecutive runs. The results demonstrate that embedding the nanoscale catalyst into the matrix of ordered mesoporous carbon remarkably extends the life of catalyst.

The magnetization curves of catalysts were investigated by vibrating sample magnetometer (VSM) at 298 K and the results were shown in Fig. 13. The corresponding magnetic parameters including saturation magnetization (M_s), remnant magnetization (M_r) and coercivity (H_c) of the samples are listed in Table 4. For

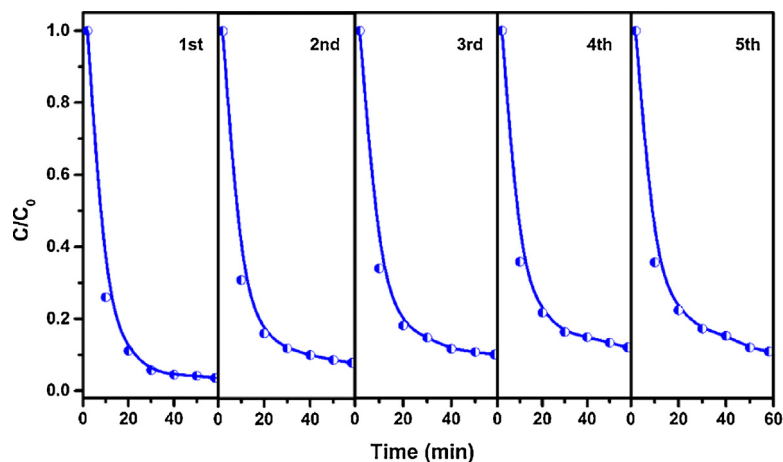


Fig. 12. Degradation of BPA in different batch runs in the H_2O_2 -CuFe-MC-1-800-BPA system.

Table 4
Magnetic properties of ordered mesoporous carbon nanocomposites.

Sample	M_s [emu g ⁻¹]	M_r [emu g ⁻¹]	H_c [Oe]
CuFe-MC-1-400	–	–	–
CuFe-MC-1-600	13.96	1.57	233.27
CuFe-MC-1-800	3.25	1.02	111.41
CuFe-MC-2-800	6.49	0.81	240.40
CuFe-MC-3-800	11.60	1.70	336.88
Fe-MC-1-800	3.54	0.40	39.55

example, the M_s , M_r and H_c of CuFe-MC-1-800 are 3.25 emu g⁻¹, 1.02 emu g⁻¹ and 111.41 Oe, respectively. The results show that M_s increased to 6.49 and 11.60 emu g⁻¹ when the Fe contents increased to 4.5 and 7.5%. The loop suggests a significant content of ferromagnetic materials. In addition, they can be easily re-dispersed for reuse after separating, because of their low M_r values [27]. The ferromagnetism shown in Fig. 13(inset) affirms that the composite catalyst could be easily separated by a magnet and reused from aqueous solution.

4. Conclusions

We demonstrated iron-copper bimetallic nanoparticles embedded within ordered mesoporous carbon composite catalyst (CuFe-MC). It was synthesized via a “one-pot” block-copolymer self-assembly strategy. TEM and SAXRD results showed that the catalyst was ordered 2D hexagonal mesostructure and iron-copper bimetallic nanoparticles highly dispersed in the matrix of ordered mesoporous carbon. Effective degradation of various robust organic contaminants was achieved by using CuFe-MC as heterogeneous Fenton catalyst. CuFe-MC showed high mineralization efficiency for phenol, benzoic acid, bisphenol A, 2,4,6-trichlorophenol, imidacloprid, ketoprofen, methylene blue and methyl orange. Besides, the TOC removal of contaminants by CuFe-MC was higher than homogeneous Fenton reagent (Fe²⁺) at the same reaction condition. For example, 94% TOC removal of imidacloprid (100 mg L⁻¹) was achieved by CuFe-MC in 12 h, while only 38% by Fe²⁺ ion. In summary, there are four remarkable advantages of composite catalyst as follows. Firstly, the high BET surface area (639 m² g⁻¹) played a major role in the adsorption of organic contaminants and the mesostructure favored rapid diffusion of reactants and products. Secondly, iron-copper bimetallic nanoparticles highly dispersed in the matrix of ordered mesoporous carbon greatly increased the amount of active sites, therefore, the contaminants molecular adsorbed on the surface of catalysts could be instantly decomposed. Thirdly, the synergistic effect of iron and copper favored the redox cycles of Fe³⁺/Fe²⁺ and Cu²⁺/Cu⁺, enhancing the catalytic activity of composite catalysts. Finally, ordered mesoporous carbon used as supporting material also can active H₂O₂ to generate •OH. The stability and recoverability of composite catalysts were assessed and showed good stability and easily to be separated using a magnet. Therefore, this magnetic composite catalyst provides a potential advantage in organic contaminants removal.

Acknowledgements

This work was supported jointly by the National Natural Science Foundation P.R. China (Project Nos. 21277099, 21207101),

Shanghai Municipal Education Commission and Shanghai Educational Development Foundation (Project No. 2011CG19).

References

- [1] E. Brillas, I. Sires, M.A. Oturan, Chem. Rev. 109 (2009) 6570–6631.
- [2] G.K. Zhang, Y.Y. Gao, Y.L. Zhang, Y.D. Guo, Environ. Sci. Technol. 44 (2010) 6384–6389.
- [3] Y.L. Zhang, K. Zhang, C.M. Dai, X.F. Zhou, H.P. Si, Chem. Eng. J. 244 (2014) 438–445.
- [4] L.J. Xu, J.L. Wang, J. Hazard. Mater. 186 (2011) 256–264.
- [5] S. Navalón, M. Alvaro, H. Garcia, Appl. Catal. B: Environ. 99 (2010) 1–26.
- [6] K.A. Sashkina, V.S. Labko, N.A. Rudina, V.N. Parmon, E.V. Parkhomchuk, J. Catal. 299 (2013) 44–52.
- [7] Y. Segura, F. Martinez, J.A. Melero, R. Molina, R. Chand, D.H. Bremner, Appl. Catal. B: Environ. 113 (2012) 100–106.
- [8] R.X. Huang, Z.Q. Fang, X.M. Yan, W. Cheng, Chem. Eng. J. 197 (2012) 242–249.
- [9] X.L. Liang, Y.H. Zhong, S.Y. Zhu, L.Y. Ma, P. Yuan, J.X. Zhu, H.P. He, Z. Jiang, J. Hazard. Mater. 199 (2012) 247–254.
- [10] Y.B. Zhao, F. Pan, H. Li, T.C. Niu, G.Q. Xu, W. Chen, J. Mater. Chem. A 1 (2013) 7242–7246.
- [11] Z.B. Han, Y.C. Dong, S.M. Dong, J. Hazard. Mater. 189 (2011) 241–248.
- [12] M. Xia, M.C. Long, Y.D. Yang, C. Chen, W.M. Cai, B.X. Zhou, Appl. Catal. B: Environ. 110 (2011) 118–125.
- [13] F.L.Y. Lam, X.J. Hu, Ind. Eng. Chem. Res. 52 (2013) 6639–6646.
- [14] M. Dukkanci, G. Gunduz, S. Yilmaz, Y.C. Yaman, R.V. Prihod'ko, I.V. Stolyarova, Appl. Catal. B: Environ. 95 (2010) 270–278.
- [15] M.N. Timofeeva, S.T. Khankhasaeva, E.P. Talsi, V.N. Panchenko, A.V. Golovin, E.T. Dashinamzhilova, S.V. Tsybulya, Appl. Catal. B: Environ. 90 (2009) 618–627.
- [16] Y.B. Wang, H.Y. Zhao, M.F.Q. Li, J.H. Fan, G.H. Zhao, Appl. Catal. B: Environ. 147 (2014) 534–545.
- [17] T. Valdes-Solis, P. Valle-Vigón, M. Sevilla, A.B. Fuertes, J. Catal. 251 (2007) 239–243.
- [18] M. Hartmann, S. Kullmann, H. Keller, J. Mater. Chem. 20 (2010) 9002–9017.
- [19] S. Navalón, A. Dhakshinamoorthy, M. Alvaro, H. Garcia, ChemSusChem 4 (2011) 1712–1730.
- [20] J. Deng, X. Wen, Q. Wang, Mater. Res. Bull. 47 (2012) 3369–3376.
- [21] Y.P. Zhai, Y.Q. Dou, X.X. Liu, B. Tu, D.Y. Zhao, J. Mater. Chem. 19 (2009) 3292–3300.
- [22] Y.P. Zhai, Y.Q. Dou, X.X. Liu, S.S. Park, C.S. Ha, D.Y. Zhao, Carbon 49 (2011) 545–555.
- [23] L.N. Kong, W. Wei, Q.F. Zhao, J.Q. Wang, Y. Wan, ACS Catal. 2 (2012) 2577–2586.
- [24] Y.X. Zhang, S.C. Xu, Y.Y. Luo, S.S. Pan, H.L. Ding, G.H. Li, J. Mater. Chem. 21 (2011) 3664–3671.
- [25] D.Y. Zhao, T. Yu, Y.H. Deng, L. Wang, R.L. Liu, L.J. Zhang, B. Tu, Adv. Mater. 19 (2007) 2301–2306.
- [26] M.E. Lindsey, M.A. Tarr, Chemosphere 41 (2000) 409–417.
- [27] T.D. Nguyen, N.H. Phan, M.H. Do, K.T. Ngo, J. Hazard. Mater. 185 (2011) 653–661.
- [28] S.H. Bossmann, E. Oliveros, S. Gob, S. Siegwart, E.P. Dahlen, L. Payawan, M. Straub, M. Worner, A.M. Braun, J. Phys. Chem. A 102 (1998) 5542–5550.
- [29] J.Y. Feng, X.J. Hu, P.L. Yue, Environ. Sci. Technol. 38 (2004) 5773–5778.
- [30] S. Wang, Q.F. Zhao, H.M. Wei, J.Q. Wang, M.Y. Cho, H.S. Cho, O. Terasaki, Y. Wan, J. Am. Chem. Soc. 135 (2013) 11849–11860.
- [31] W. Wang, H.Y. Wang, W. Wei, Z.G. Xiao, Y. Wan, Chem. Eur. J. 17 (2011) 13461–13472.
- [32] Q. Liao, J. Sun, L. Gao, Colloid Surf. A 345 (2009) 95–100.
- [33] X.J. Yang, X.M. Xu, J. Xu, Y.F. Han, J. Am. Chem. Soc. 135 (2013) 16058–16061.
- [34] X.J. Yang, P.F. Tian, C.X. Zhang, Y.Q. Deng, J. Xu, J.L. Gong, Y.F. Han, Appl. Catal. B: Environ. 134 (2013) 145–152.
- [35] S. Malato, J. Caceres, A. Agüera, M. Mezcuá, D. Hernando, J. Vial, A.R. Fernández-Alba, Environ. Sci. Technol. 35 (2001) 4359–4366.
- [36] H.Y. Zhao, J.L. Cao, H.L. Lv, Y.B. Wang, G.H. Zhao, Catal. Commun. 41 (2013) 87–90.
- [37] W. Luo, L.H. Zhu, N. Wang, H.Q. Tang, M.J. Cao, Y.B. She, Environ. Sci. Technol. 44 (2010) 1786–1791.
- [38] S. Luo, S.G. Yang, C. Sun, X.D. Wang, Water Res. 45 (2011) 1519–1528.
- [39] X.Y. Zhang, Y.B. Ding, H.Q. Tang, X.Y. Han, L.H. Zhu, N. Wang, Chem. Eng. J. 236 (2014) 251–262.
- [40] Z.L. Hua, W.Q. Ma, X. Bai, R.R. Feng, L. Yu, X.Y. Zhang, Z.Y. Dai, Environ. Sci. Pollut. Res. 21 (2014) 7737–7745.
- [41] ChemIDplus Adv, Specialized Information Services, <http://chem.sis.nlm.nih.gov/chemidplus/>
- [42] N. Lu, Y. Lu, F.Y. Liu, K. Zhao, X. Yuan, Y.H. Zhao, Y. Li, H.W. Qin, J. Zhu, Chemosphere 91 (2013) 1266–1272.
- [43] Y. Segura, F. Martinez, J.A. Melero, Appl. Catal. B: Environ. 136 (2013) 64–69.
- [44] L.L. Zhang, Y.L. Nie, C. Hu, J.H. Qu, Appl. Catal. B: Environ. 125 (2012) 418–424.